THE JOURNAL OF PHYSICAL CHEMISTRY C
A JOURNAL OF THE AMERICAN CHEMICAL SOCIETY

pubs.acs.org/JPCC

Article

Gas-Phase Photocatalytic CO_2 Methanation over Ru/TiO_2: Effects of Pressure, Temperature, and Illumination

Alondra M. Ortiz-Ortiz,[‖] Carissa S. Yim,[‖] Daniel O. Delgado Cornejo, Andrew J. Gayle, Alexander J. Hill, Victor A. Vogt, Daniel W. Liao, Thomas Coons, Galen B. Fisher,* Andrej Lenert,* Johannes W. Schwank,* and Neil P. Dasgupta*

Cite This: *J. Phys. Chem. C* 2024, 128, 18284−18292

Read Online

ACCESS | Metrics & More | Article Recommendations | Supporting Information

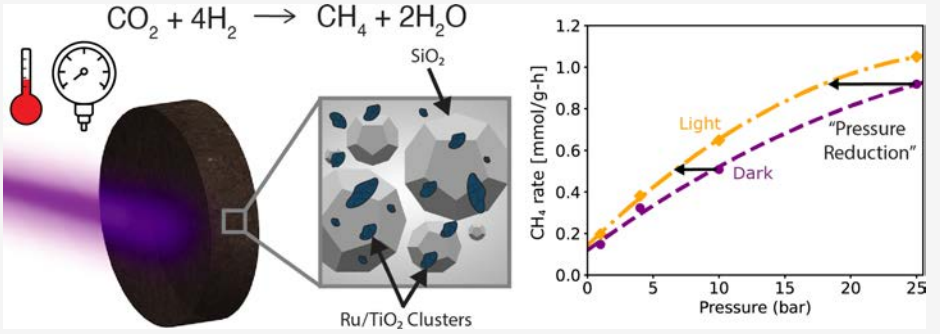

ABSTRACT: This work examines the effects of temperature (100−150 °C), pressure (1−25 bar), and UV illumination on gas-phase photocatalytic CO_2 methanation over Ru/TiO_2. Irradiating the catalyst enables an ∼20% decrease in operating pressure to maintain the same production rate. Furthermore, the relative light enhancement is greater at 100 °C than 150 °C—a phenomenon attributed to increased carrier recombination rates at higher temperatures. Arrhenius experiments indicate that the global activation energy (E_a) of the reaction is similar in the dark and light, suggesting that rate enhancements are determined by changes in surface coverage. To test this hypothesis, the CO_2 reduction mechanism is probed using *in situ* diffuse reflectance infrared Fourier transform spectroscopy (DRIFTS). The spectra show an increase in the relative surface coverage of the intermediate formyl group under irradiation. These findings illustrate that, within the experimental conditions explored in this study, the photoexcitation of charge carriers in the semiconductor primarily influences the surface coverage of intermediates to drive enhanced methane formation at low temperatures.

1. INTRODUCTION

One approach to both limit greenhouse gases and provide a hydrogen-dense fuel is the conversion of CO_2 to methane (CH_4, eq 1).[1−3] If the hydrogen reactant is produced using renewable electricity, this allows sustainable conversion of CO_2 to a widely used and versatile fuel. However, methanation of CO_2, known as the Sabatier reaction, is an energy-intensive, thermal catalytic process that is commonly executed at high temperatures (300−550 °C) and at pressures up to 100 bar.[4,5]

$$CO_2 + 4H_2 \rightarrow CH_4 + 2H_2O \quad (1)$$

Among various approaches being explored to enhance the Sabatier reaction, photocatalytic CO_2 methanation mediated by a semiconducting material that absorbs light and generates electron−hole pairs is a promising option.[6−10] The rate of chemical reactions in semiconductor photocatalysts may be influenced by the equilibrium concentration of charge carriers under illumination as well as changes to the surface chemical adsorption/desorption and reaction mechanisms.

Metal cocatalysts are commonly paired with semiconductors to enhance turnover frequency at surface reaction sites and may also facilitate charge separation at the metal/semiconductor interface.[8,11−16] For this purpose, a variety of metals including Ru,[17−19] Rh,[20] Ni,[21] and Pt,[22] among others, have been explored at a range of temperatures from 100 to 400 °C for heterogeneous, gas-phase photocatalytic CO_2 methanation.[6,23,24] Photocatalytic studies of the Sabatier reaction have typically been carried out near atmospheric pressure, with a maximum reported pressure of 8 bar.[25] Light-driven gas-phase CO_2 methanation has not been extensively studied in higher pressure environments. Prior work has attributed the

Received: August 25, 2024
Revised: September 30, 2024
Accepted: October 2, 2024
Published: October 18, 2024

observed enhancement in reaction rate to a variety of phenomena including photothermal heating,[23,26] plasmonic resonance,[20,27,28] and direct hot-electron injection into adsorbed CO_2.[4,24] As such, a detailed understanding of the coupled effects of light and heat on the reaction pathways and kinetics of the Sabatier reaction requires further investigation.

In this work, we investigate the synergistic effects of altering temperature (100−150 °C), pressure (1−25 bar), and UV illumination on the gas-phase, photocatalytic methanation of CO_2. To study the reaction mechanism at low temperatures, we selected Ru because it is among the most active thermal catalysts for CO_2 methanation reported in the literature.[3,6,18,24,29,30] Similarly, TiO_2 is one of the most widely used semiconductors for a variety of photocatalytic reactions including CO_2 methanation due to its photoactivity, stability, low cost, and earth abundance.[7,10,30−32] Thus, we use Ru/TiO_2 as a model material system to study the mechanism of photocatalytic CO_2 methanation.

Through Arrhenius analysis and *in situ* DRIFTS, we observe no significant difference between the dark and light reaction pathways and activation energies. Instead, UV illumination impacts the kinetics of reaction intermediate formation, which suggests that a change in the relative concentration of surface intermediates is the primary factor that influences the observed increase in CH_4 production rate. We further demonstrate that the enhancement from illumination is not purely a thermal effect and is deactivated at longer wavelengths of light (below the bandgap of TiO_2). The relative increases in reaction rate under illumination are more pronounced at lower reaction temperatures, which is attributed to the temperature-dependence of charge carrier recombination.[33] The understanding presented here can inform the design of future photocatalysts that harness light-mediated surface coverage effects to efficiently transform CO_2 into fuels.

2. METHODS

2.1. Ru/TiO_2 Nanoparticle Fabrication. Ru-loaded TiO_2 (Ru/TiO_2, 4 wt % Ru) nanoparticles (NPs) are prepared using wet impregnation according to a previously reported procedure.[34] 2.0 g of TiO_2 (Aeroxide P25, Fisher Scientific) is suspended in 41 mL of deionized (DI) water under vigorous stirring. A second mixture of 0.1642 g of $RuCl_3{\cdot}3H_2O$ (99.9%, ACROS Organics, Fisher Scientific) in 9 mL of DI water is prepared and inserted into an ultrasonic bath. The second mixture is added to the first mixture, and the pH is adjusted to 7 using NaOH. The solution is evaporated until it is dry at 50 °C under continuous stirring. This is followed by drying at 110 °C overnight. The dry sample is ground into a powder and reduced in forming gas (5% H_2, balance N_2) at 300 °C for 3 h to convert the $RuCl_3$ NPs to Ru metal NPs.

2.2. Catalyst Loading. A quartz frit with a characteristic pore size of 40−90 μm, a diameter of 10 mm, and a thickness of 2−3 mm (Technical Glass Products) is used as a transparent support material. The quartz frit is chosen as a wide-bandgap substrate that will increase the light-exposed surface area and promote more uniform illumination of the catalytically active material. The quartz frit is cleaned by sonication sequentially in 1 M HCl and DI water for 5 min each, followed by drying for 1 h at 110 °C in air. Ru/TiO_2 is loaded into the quartz frit using wet impregnation with a solution containing 2 mL of DI water, 12 mL of methanol, and 100 mg of Ru/TiO_2. The solution is immersed in an ultrasonic bath for 1 h. A magnetic stir bar and fixture housing the quartz frit are placed into the beaker. The fixture prevents excessive settling of Ru/TiO_2 onto the top of the quartz frit. The solution is stirred for 1 h at a speed of 1000 rpm. The quartz frit is then removed and dried at 110 °C in air for 1 h. This is followed by reduction in forming gas (5% H_2, balance N_2) for 24 h at 200 °C to ensure the complete conversion to Ru metal.[35] A schematic of the catalyst-loaded quartz frit is shown in Figure 2.

2.3. Optical and Structural Characterization. Optical microscopy images are collected using a VHX-7000 4K digital microscope (Keyence). Scanning electron microscopy (SEM) images are collected using a TESCAN MIRA3 FEG SEM with an accelerating voltage of 5 kV. To prepare samples for high-angle annular dark field scanning transmission electron microscopy (HAADF-STEM), the 4 wt % Ru/TiO_2 catalyst is dropcast onto Cu mesh grids. HAADF-STEM is performed on a Thermo Fisher Talos F200X G2 S/TEM, operated at 200 kV with an X-FEG, high-brightness Schottky-type emission gun as the electron source. A Super-X windowless EDS detector is used for EDS mapping. The Ru particle size is determined using ImageJ software. The transmittance and reflectance of the Ru/TiO_2-loaded quartz frit are measured by using a UV−vis−NIR spectrophotometer with an integrating sphere attachment (Shimadzu, Model UV-2600). X-ray photoelectron spectroscopy (XPS) is conducted using a Kratos Axis Ultra XPS with a monochromatic Al X-ray source operating at 10 mA and 12 kV. The pass energy is 40 eV, with a dwell time of 60 s. XPS spectra are normalized to the adventitious carbon (C 1s) binding energy (284.8 eV) and deconvoluted in the CasaXPS software using the Gaussian−Lorentzian-like fit, which is also supported in the literature (Supplementary Note #1). The Brunauer−Emmett−Teller (BET) surface area was determined using a Micromeritics ASAP 2020. The samples were degassed at 350 °C for 8 h prior to surface area measurements, which were conducted at 77 K.

2.4. Catalytic Activity Characterization. A custom batch reactor (Series 4793, Parr) capable of reaching temperatures up to 225 °C and pressures of up to 40 bar, equipped with a 12.7 mm diameter exposed quartz window, is used to probe the reaction rate using various reaction inputs. The reactor volume is ∼110 mL. The exterior of the reactor is heated, and the reactor temperature is controlled using a PID controller. The Ru/TiO_2-loaded quartz frit is held in front of the window inside the reactor. The same photocatalyst-loaded frit was used throughout the study to avoid discrepancies from the random distribution of the Ru/TiO_2 catalyst on the frit during solution deposition. The catalyst is illuminated with either a UVP Blak-Ray B-100AP High-Intensity UV Inspection Lamp (Fisher Scientific, intensity = 48 W/m^2) or a high-power LED (M375L4, Thorlabs, intensity = 430 W/m^2) with an emission peak at 365 nm. A thermocouple is positioned at the backside of the catalyst frit to measure the reported reaction temperature. To determine the temperature of the gas, the same thermocouple was moved out of contact with the frit during a separate experiment under the same conditions. To estimate the light-induced temperature increase of the front surface of the frit relative to the backside of the catalyst frit, a continuum-level heat transfer model is used (Supplementary Note #6). By this estimate, LED irradiation increases the front-surface temperature of the catalyst frit by less than 0.6 and 0.058 K, using the 365 nm LED or Hg lamp, respectively (relative). The output of the LED is collimated with an aspheric condenser lens (ACL2520U-DG6-A, Thorlabs) to illuminate the entire sample area. For both light sources, the

https://doi.org/10.1021/acs.jpcc.4c05724
J. Phys. Chem. C 2024, 128, 18284−18292

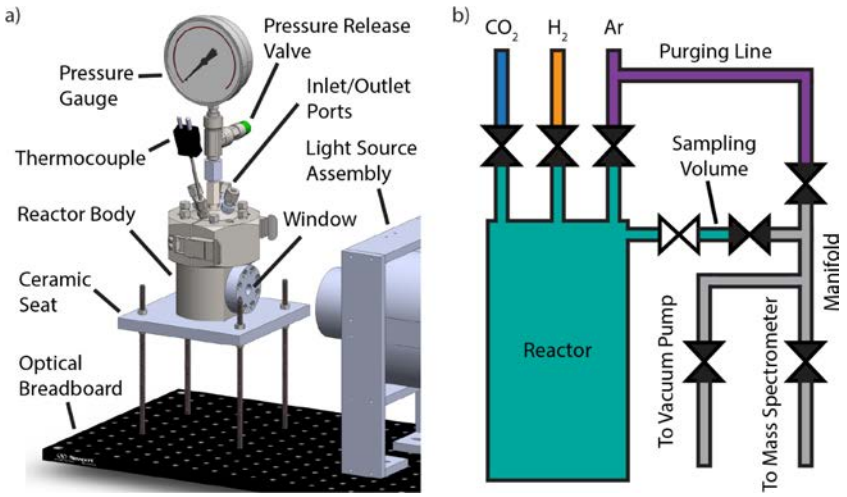

Figure 1. (a) CAD model of the reactor and the light source assembly. The black polycarbonate enclosure and gas lines connected to the reactor are not shown. (b) Scheme showing the gas line connections in the reactor system. This scheme specifically shows the moment when a small sample is taken from the reactor, within the sampling volume.

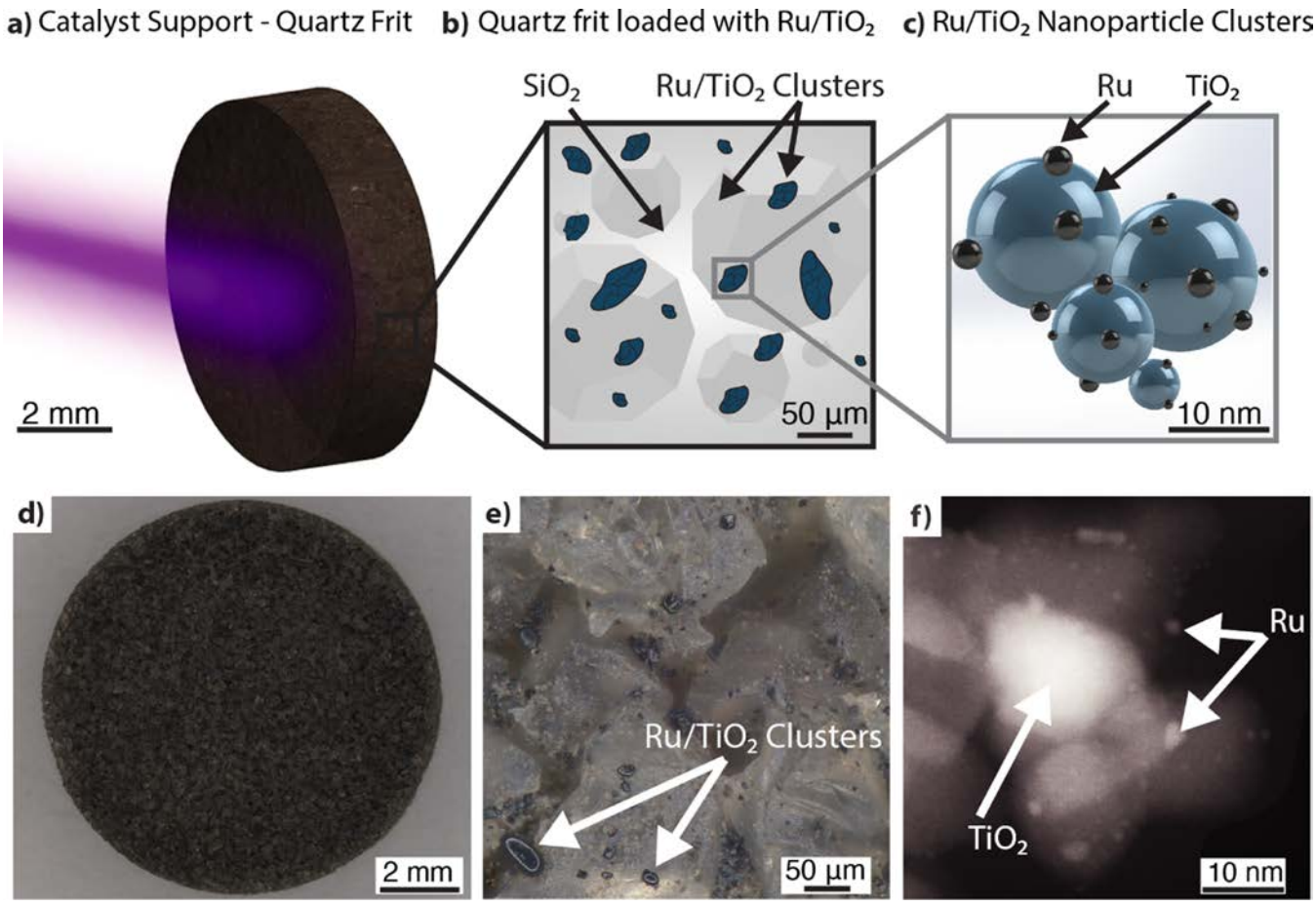

Figure 2. (a) Schematic showing the catalyst support, which is a porous quartz frit loaded with Ru/TiO_2 particles under UV light illumination. (b) Schematic showing the presence of Ru/TiO_2 clusters on the surface of the frit at the microscale. (c) Schematic showing the nanoscale geometry of the Ru/TiO_2 clusters, which consist of Ru and TiO_2 nanoparticles. (d) Optical microscopy image of quartz frit. (e) Optical microscopy image at higher magnification showing the Ru/TiO_2 clusters, which are dark in appearance. (f) HAADF-STEM image of Ru/TiO_2 powder. The larger particles are TiO_2, while the smaller particles are Ru.

same distance between the light source and sample is used, and the light intensity is measured using a GaP photodiode (Thorlabs) inside the reactor prior to testing. Further details about the calibration process can be found in Supplementary Note #2.

The interior reactor temperature is measured using a thermocouple in contact with the backside of the quartz frit.

https://doi.org/10.1021/acs.jpcc.4c05724
J. Phys. Chem. C 2024, 128, 18284−18292

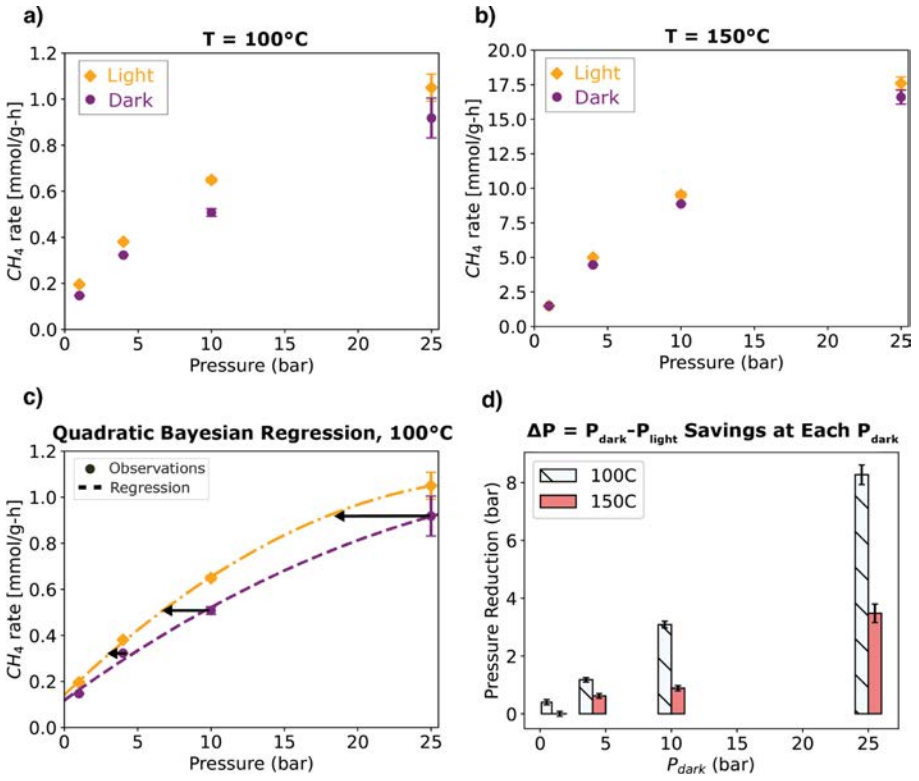

Figure 3. Reported CH_4 rates as a function of pressure at temperatures of (a) 100 °C and (b) 150 °C in terms of the total catalyst mass (only the Ru/TiO_2). Different *y*-axis scales are used in panels (a,b). The error bars on some of the data points (1−10 bar) are small enough that they are contained within the symbol. (c) Quadratic fit to rate data at 100 °C. Arrows indicate the decrease in pressure enabled by irradiation to achieve the equivalent dark rate. The R^2 values for the light and dark curves are 0.9996 and 0.9959, respectively. (d) Decrease in required pressure under irradiation to achieve the equivalent dark rate at 100 and 150 °C. Error bars in panel (d) represent ±1 standard deviation.

To limit UV exposure, the reactor and light source are covered with a black polycarbonate enclosure screwed onto the optical breadboard as part of the experimental setup shown in Figure 1a. A computer-aided design (CAD) model of the reactor and lamp is shown in Figure 1a.

The reactor is charged with gases at the beginning of each experiment, including ultrahigh-purity (UHP) Ar (99.999%), UHP H_2 (99.999%), and research laser grade CO_2 (99.999%) until the desired partial pressure of each gas is present in the reactor. A partial pressure ratio for CO_2:H_2 of 3:7[25] is used in all cases. This ratio was chosen based on a study by Kawamura *et al.* (2017), who found that CO_2 methanation rates increase with increasing P_{H2}; however, concentrations of H_2 exceeding 70% hinder CO_2 adsorption.[25]

A schematic illustration of the reactor and gas lines is shown in Figure 1b. To evaluate the composition of the gas mixture inside the reactor, a small sample (∼1 mL) is isolated from the reactor between two valves (further details about the sampling process can be found in Supplementary Note #2). To allow time for diffusive mixing of the gases and detectable levels of CH_4 formation, the first sample is taken at 90 min following the start of the reaction. Four total samples are taken at 45 min intervals. The reaction rate is calculated using a linear fit of the CH_4 formation relative to Ar by comparing the m/z 15 signal to the m/z 20 signal. Only the last three data points, where good mixing had been achieved, are used to calculate the rate.

2.5. Mass Spectrometry. A quadrupole mass spectrometer is used to measure the formation rate of CH_4. The electron energy is 70 eV, and the emission current is 100 μA. The spectra were collected in the following m/z ratio windows: m/z 3−39, m/z 41−43, and m/z 45−100. H_2, CH_4, Ar, and CO_2 are evaluated by monitoring m/z 3, 15, 20, and 22, respectively. This choice of m/z values uses unique daughter peaks for each species (*e.g.*, 3 m/z = hydrogen deuteride (HD)) so that the chosen scanning ranges do not result in detector saturation. Between samples, the mass spectrometer is flushed using Ar, while still under high vacuum, to assist in the removal of residual gases from the sample.

2.6. *In Situ* Diffuse Reflectance Infrared Fourier Transform Spectroscopy (DRIFTS). *In situ* DRIFTS is conducted using a Tensor 27 FT-IR spectrometer with an MCT detector (Bruker). At the start of each experiment, the catalyst undergoes 5 pump/purge cycles at a temperature of 315 °C, during which N_2 is flushed over the catalyst and then pumped out of the chamber. Subsequently, the catalyst is treated at 315 °C in 80 sccm of 5% H_2/N_2 for 1 h, and is then cooled to 125 °C in N_2. CO_2 and H_2 (3:7 ratio) are sequentially fed into the chamber until a total gauge pressure of 1 bar is achieved, and then the chamber is sealed to create a batch environment. Spectra are gathered in 60 s intervals by averaging 45 scans with a resolution of 4 cm^{-1} for 5 h to match the duration of a batch CO_2 reduction reaction. For light-on tests, the catalyst is irradiated with a 365 nm Thorlabs LED (M365LP1) at 430 W/m^2 for the duration of the experiment.

3. RESULTS AND DISCUSSION

3.1. Structural and Optical Characterization. Figure 2a shows the experimental platform that was used to investigate various reaction conditions, including variations in temperature, pressure, and light intensity. The catalyst is loaded onto

https://doi.org/10.1021/acs.jpcc.4c05724
J. Phys. Chem. C 2024, 128, 18284−18292

a transparent, porous quartz frit substrate, which was selected to increase the surface area and promote a more uniform illumination of the catalytically active material. This quartz frit was loaded with Ru/TiO_2 NPs that coalesced into clusters on the surface of the frit (Figure 2b,c). Figure 2d,e shows optical microscopy images of the quartz frit support following Ru/TiO_2 loading. As shown in Figure 2b,e, at higher magnifications, the clusters of Ru/TiO_2 vary in size from one to tens of micrometers.

HAADF-STEM imaging is used to visualize the Ru nanoparticle size and distribution along the surface of the TiO_2 nanoparticles prior to loading them onto the quartz frit (Figure 2c,f). The larger particles are P25 TiO_2, while the smaller, lighter-shaded particles are Ru. The distribution of Ru NPs along the surface of P25 TiO_2 is relatively uniform, with an average particle size of ∼2 nm (Figure S1). UV−vis spectrophotometry measurements indicate an increase in light absorption after loading Ru/TiO_2 onto the quartz frit (Figure S2).

Additionally, as determined by BET analysis, the surface areas of the bare TiO_2 powder and the Ru/TiO_2 powder are 55.5 and 53.3 m^2/g, respectively. BET analysis of the bare quartz frit was also attempted; however, the surface area is below the measurable threshold of the instrument, indicating that the majority of the surface area of the catalyst is attributed to the Ru/TiO_2 powder and not the quartz frit substrate. Overall, these structural and optical properties suggest that the Ru/TiO_2-loaded quartz frit is an appropriate platform for investigating photocatalytic CO_2 methanation, wherein the distribution of the Ru/TiO_2 along the surface of the quartz frit increases the catalyst surface area that is accessible to illumination.

3.2. Photocatalytic Activity Characterization. To study the effects of temperature, pressure, and UV-illumination on the CH_4 production rate, the methanation activity of the Ru/TiO_2-based catalyst is measured at 100 and 150 °C, while pressure is varied from 1 to 25 bar. The same photocatalyst-loaded quartz frit was used for each experiment, as described in Section 2.4. A summary of the photocatalytic activity for CO_2 methanation is shown in Figure 3.

Figure 3a shows the dark and light CH_4 production rates as a function of pressure at a temperature of 100 °C. At all pressures, illumination is observed to increase the rate. Additionally, as the pressure increases, the reaction rate monotonically increases. Increasing pressure increases the reactant surface coverage as well as the likelihood of reactant collision and conversion. Equilibrium also favors the forward reaction at a higher pressure. These factors led to greater methane formation rates.

In Figure 3b, similar trends are observed when the temperature is increased to 150 °C, although light enhancement at 1 bar was negligible. The calculated percentage light enhancement for all conditions can be found in Figure S6 and Supplementary Note #3. The overall reaction rates are higher at 150 °C than at 100 °C. However, while the absolute increase in rate under illumination is greater at 150 °C (for a given pressure), the relative enhancement (as a percentage of the dark rate) is diminished at the higher temperature. Previous observations of gas-phase photocatalysis for ethylene oxidation over TiO_2 have also reported a decreased enhancement at elevated temperatures, which was attributed to increased carrier recombination rates in the TiO_2 semiconductor.[36] To gain a better understanding of these effects in our model system, *in situ* DRIFTS experiments are carried out and will be discussed in Section 3.4.

Figure 3c shows a Bayesian quadratic polynomial regression model fit to the methanation rates at 100 °C in the dark and light. The trend lines illustrate that irradiation of the catalyst reduces the pressure necessary to achieve an equivalent dark methanation rate. The decrease in required pressure to achieve an equivalent dark rate, referred to as "pressure reduction", is shown in Figure 3d, along with ± one standard deviation error bars, as computed *via* the Bayesian regression uncertainty. Supplementary Note #4 provides the fitted rate *versus* pressure data collected at 150 °C and further details of the regression model. The pressure reduction is more significant at lower temperatures as absolute pressure increases.

Overall, Figure 3 demonstrates that for photocatalytic methanation over Ru/TiO_2, illumination can reduce the pressure requirements by ∼20% to achieve the same rate for the Sabatier reaction. The peak rate of >15 mmol $CH_4/g_{cat}/h$ (Figure 3a) is comparable to many recent reports of photoenhanced CO_2 reduction,[4,24,25,37−39] aside from studies that report a higher production rate but attribute it to photothermal heating of the metal.[23,37]

The results above demonstrate substantial pressure reductions under illumination and suggest that the photoexcited charge carriers in the TiO_2 semiconductor facilitate CO_2 methanation. To help rule out purely light-induced heating, we replaced the broadband light source (Hg lamp) with a UV light-emitting diode (LED) (Thorlabs, M365LP1). The peak emission of the LED is 365 nm, or approximately 3.4 eV, which exceeds the bandgap energy of P25 TiO_2 (∼3.2 eV). Using monochromatic 365 nm illumination, we observe an enhanced methanation rate that monotonically increases with light intensity (see Supplementary Note #4 for discussion and further statistical analysis). In contrast, when below-bandgap illumination is used (450 nm or 2.76 eV, Thorlabs LED MNWHL4f), no rate enhancement is observed (see Supplementary Note #5), despite comparable light absorption observed using UV−vis at 450 and 365 nm (Supplementary Note #1). This provides evidence that the mechanism of light enhancement involves the generation of electron−hole pairs in the semiconductor, rather than a purely thermal effect.

Additional control experiments using the identical P25 TiO_2 catalyst without a Ru cocatalyst showed negligible methane production within the noise floor of the mass spectrometer under both dark and light conditions at 10 bar and 125 °C. This demonstrates that the synergy between Ru and TiO_2 is necessary to drive a significant rate of CH_4 production under our experimental conditions. Therefore, to further probe the mechanism responsible for the measured light enhancement, we performed additional experiments to determine the apparent activation energy and monitor surface intermediates (*via in situ* DRIFTS).

3.3. Light-Enhancement Mechanism. Temperature-dependent rate measurements are conducted to investigate whether UV illumination impacts the activation energy (E_a) for CH_4 formation (Figure 4). The reaction is evaluated at 110, 125, and 140 °C under 365 nm LED irradiation at 100% light intensity (430 W/m^2).

Figure 4 shows the CH_4 production rates in light and dark conditions at 10 bar as a function of the temperature. At 110, 125, and 140 °C, the dark rates were 0.13, 0.47, and 1.2 mmol/g·h, respectively, which increased to 0.16, 0.55, and 1.4 mmol/g·h under illumination. In Figure 4, a vertical shift is observed

https://doi.org/10.1021/acs.jpcc.4c05724
J. Phys. Chem. C 2024, 128, 18284−18292

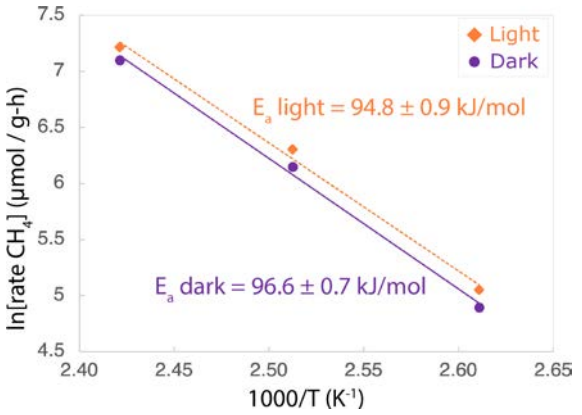

Figure 4. Arrhenius plot of CO_2 methanation over Ru/TiO_2 at 110, 125, and 140 °C under a pressure of 10 bar, with and without 365 nm irradiation (430 W/m^2). The error in the activation energy values reflects a 90% confidence interval on the fit.

under illumination, indicating an increase in activity. At 110 °C, the observed CH_4 rate is 0.13 mmol/g·h for dark conditions. Under illumination, the CH_4 rate increases by 23% to 0.16 mmol/g·h, which is consistent with the results in Figures 3 and S6. Nevertheless, similar activation energies were observed with and without irradiation (94.8 and 96.6 kJ/mol, respectively) suggesting that the photocatalytic and dark (pure thermal) reaction rates are governed by the same rate-determining step.[40]

We note that in this study the catalyst material, geometry, and loading were not optimized to maximize the rate enhancements. Therefore, in the future, we anticipate that the relative enhancement could be increased further by optimizing the catalyst architecture (*i.e.*, composition, geometry, distribution) and ultimately the rate enhancement, which can enable decoupling of absorption and surface kinetic parameters.[41]

Nonetheless, the results from this study demonstrate that illumination of the photocatalyst with above-band gap light produces an enhancement in the catalytic activity, which cannot be explained by purely thermal effects. Furthermore, the measured activation energies suggest that there is no significant difference in the overall reaction pathways under illumination. This, in turn, suggests that the rate enhancement under illumination is a result of changes in the pre-exponential factor of the rate equation, which is associated with collision probabilities and frequencies. Therefore, *in situ* DRIFTS is performed to probe the hypothesis that light irradiation affects the relative surface coverage of reaction intermediates during the CO_2 methanation reaction.

3.4. *In Situ* DRIFTS. Figure 5 provides a schematic of CO_2 methanation pathways, alongside the *in situ* DRIFTS spectra that were used to probe the light-enhancement mechanism of methanation of CO_2 to CH_4 over the Ru/TiO_2 catalyst.

There are two established pathways for CO_2 methanation shown in Figure 5a. In the dissociative pathway, CO_2 adsorbs on the catalyst to form CO before it is reduced, whereas in the direct pathway, CO_2 absorbs and is directly hydrogenated to methane.[42,43] Alternative CO_2 conversion pathways exist, including the reverse water-gas shift (RWGS) reaction, which would lead to the combined generation of CO and CH_4. However, the low reaction temperatures studied herein are not conducive to the RWGS reaction.[18] To study the influence of light on the methanation pathway over Ru/TiO_2, *in situ* DRIFTS experiments are performed at 125 °C and 1 bar (3:7 ratio CO_2:H_2) according to the methods described in Section 2.6. Dark and light reaction conditions were tested separately on the same catalyst sample using a cleaning cycle between experiments. The cleaning procedure removes adsorbates (such as OH or hydrocarbons) that formed during the previous reaction from the Ru/TiO_2 surface as corroborated through a DRIFTS scan (Supplementary Note #7).

Figure 5b compares the DRIFTS spectra under dark and illumination conditions for the CO_2 methanation experiments over Ru/TiO_2. The broad band centered at 3250 cm^{-1} corresponds to surface hydroxyl (OH) groups. Formyl (HCO, 1865 cm^{-1}), carbonate (CO_3^{2-}, 1645 cm^{-1}), and formate groups (HCOO, 1540 and 1400 cm^{-1}) are also

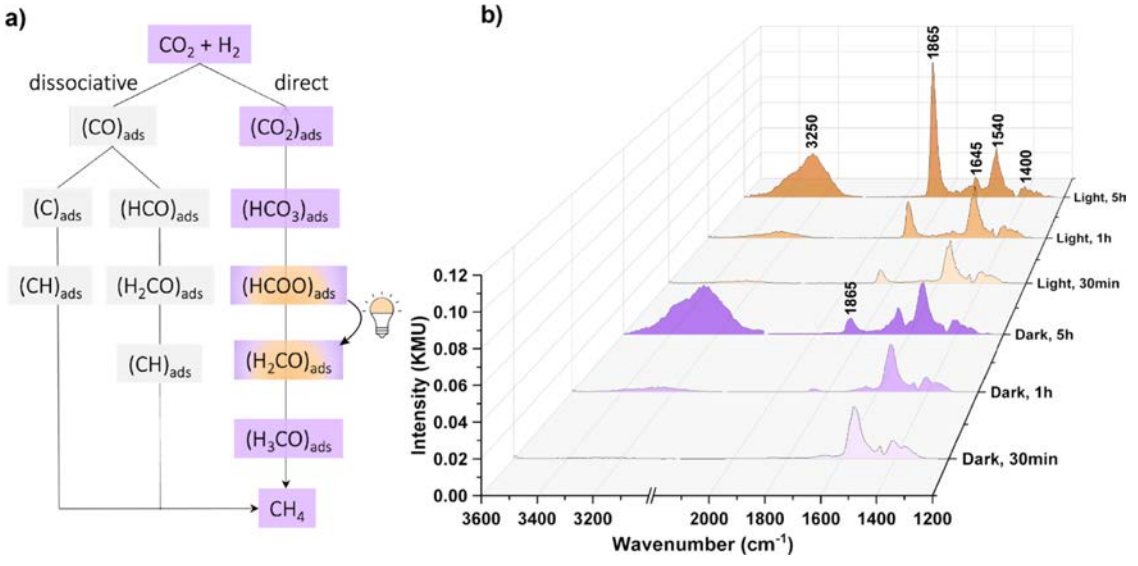

Figure 5. (a) Diagram of two possible CO_2 reduction pathways. (b) *In situ* DRIFTS spectra at 125 °C and 1 bar with and without 365 nm irradiation at 430 W/m^2. Light and dark experiments are executed on the same catalyst independently on different days with identical pretreatments to clean the catalyst surface between experiments.

https://doi.org/10.1021/acs.jpcc.4c05724
J. Phys. Chem. C 2024, 128, 18284−18292

prominent on the Ru/TiO_2 surface.[44] From literature, the 2000−2100 cm^{-1} region is assigned to CO adsorbed on Ru or at the Ru/TiO_2 interface.[34,45] In Figure 5b, there are no peaks from 2000 to 2100 cm^{-1}, showing that CO_2 is directly hydrogenated to hydrocarbons and is subsequently reduced to CH_4 over Ru/TiO_2. Thus, under our experimental conditions, the direct pathway, rather than the dissociative hydrogenation pathway, is favored both in the dark and under illumination (Figure 5a).

In Figure 5b, the progressive increase with time in the abundance of formate (1540 and 1400 cm^{-1}), carbonate (1645 cm^{-1}), and hydroxyl (3250 cm^{-1}) intermediates is comparable under both dark and light conditions. However, within the first 30−60 min, formyl groups (1865 cm^{-1}) appear under illumination and are significantly more abundant after 5 h of light exposure compared with dark conditions. The difference in the relative abundance of the formyl intermediate suggests that the light-accelerated step is the cleavage of an oxygen from formate (HCOO) to generate formyl (HCO) species. Additionally, the growth of the formyl group cannot be explained by light-induced heating alone (refer to Supplementary Note #7). The *in situ* DRIFTS analysis indicates that light primarily influences the relative concentration of surface intermediates to accelerate the rate of CO_2 methanation over Ru/TiO_2.

The DRIFTS spectra further support the hypothesis that photoexcited charge carriers in TiO_2 play a role in rate enhancement, rather than purely light-induced heating of the Ru nanoparticles (refer to Supplementary Note #7). Ru NPs are thought to facilitate H_2 dissociation, subsequent migration to the support (spillover), and OH group formation.[46] A comparison of XPS spectra on our catalyst before and after the reaction indicates that the abundance of oxidized Ru significantly decreases in the postmortem XPS spectra, suggesting that Ru sites were reduced after repeated methanation reactions (refer to Supplementary Note #1, Figure S4). On the other hand, carbonates, formates, and formyl intermediates form on bare TiO_2 when it is exposed to CO_2 and H_2.[29] Therefore, the similar OH group abundance (related to H_2 splitting on Ru), contrasted with the significant difference in hydrocarbon coverage (related to the bare TiO_2 or Ru/TiO_2 interface) in the dark and under irradiation, is evidence that photogenerated charge carriers in the semiconductor may migrate to Ru sites to enhance the methanation rate of CO_2 at low temperature and pressure. This is analogous to a recent study by Qin *et al.* of CO conversion to hydrocarbons over a $Ni-TiO_2$ catalyst, which proposed that C−C coupling is accelerated under illumination by the migration of photogenerated electrons from TiO_2 to Ni sites, influencing the surface coverage of CH intermediates.[47] Overall, the DRIFTS analysis provides valuable mechanistic insights into the origins of photoenhancement of the reaction rate, which is attributed to light-induced changes to the surface coverage of reaction intermediates. The DRIFTS results also indicate negligible CO formation over the Ru/TiO_2 photocatalyst.

4. CONCLUSIONS

This study investigates the combined effects of illumination, temperature, and pressure on gas-phase CO_2 methanation over Ru/TiO_2 using a versatile photoreactor capable of operating at a wide range of pressures (1−25 bar) and temperatures (100−150 °C). A Ru/TiO_2 loaded quartz frit is used as a model catalyst system. Exposure of the photocatalyst to UV irradiation resulted in an increase in the catalyst activity and a decrease in the pressure requirements to achieve reduction of CO_2 to CH_4. Over a range of pressures, the observed percentage of light enhancement is more pronounced at 100 °C than 150 °C. Since the charge carrier recombination rate is known to increase at elevated temperatures, the greater percent enhancement at lower temperature indicates that photoexcited carriers influence the CO_2 reduction process. To further support this claim, when a monochromatic LED with a wavelength above the bandgap of the TiO_2 semiconductor is used, rate enhancement is observed. In contrast, no statistically significant difference in the reaction rate is observed using below-bandgap illumination, confirming that the enhancement is driven by charge carriers excited within the semiconductor.

To probe the light-enhancement reaction mechanism, Arrhenius analysis was performed to quantify the temperature-dependent activity in the dark and light. Similar activation energies were observed in dark and light conditions, indicating that illumination does not change the rate-limiting step.

Collectively, these results point toward a change in the preexponential factor of the rate equation. To test this hypothesis, *in situ* DRIFTS reveals that CO_2 is directly hydrogenated to CH_4 over Ru/TiO_2 without a CO intermediate, and light increases the surface concentration of the formyl (H_2CO) intermediate species from formate (HCOO) *via* oxygen cleavage. Therefore, the DRIFTS analysis provides evidence that the rate enhancement is a result of light-induced changes in the relative concentration of surface intermediates.

We envision that this work will provide a better understanding of the reaction mechanisms of CO_2 methanation and inform the design of future photocatalysts that harness the use of light-mediated surface coverage to accelerate the transformation of CO_2 into fuels. From a practical implementation standpoint, these insights can be used to guide future system design of modular, photocatalytic CO_2 conversion reactors, where process parameters such as pressure, temperature, and illumination can be synergistically optimized to maximize performance and energy efficiency. A better understanding of the interplay between these process parameters can help promote distributed generation of fuels in a variety of contexts or settings while mitigating rising concerns in supply chains.

■ ASSOCIATED CONTENT

Supporting Information

The Supporting Information is available free of charge at https://pubs.acs.org/doi/10.1021/acs.jpcc.4c05724.

Catalyst characterization including particle size analysis, UV−vis, optical image, XPS spectra and fitting parameters; description of calibration and reaction sampling procedure; statistical regression models, light enhancement, reproducibility measurements, and light intensity trends; wavelength dependence test to decouple the role of Ru/TiO_2; heat transfer model description and results; additional DRIFTS experimental details (PDF)

https://doi.org/10.1021/acs.jpcc.4c05724
J. Phys. Chem. C 2024, 128, 18284−18292

AUTHOR INFORMATION

Corresponding Authors

Galen B. Fisher − *Department of Chemical Engineering, University of Michigan, Ann Arbor, Michigan 48109, United States*; Email: gbfisher@umich.edu

Andrej Lenert − *Department of Chemical Engineering, University of Michigan, Ann Arbor, Michigan 48109, United States*; orcid.org/0000-0002-1142-6627; Email: alenert@umich.edu

Johannes W. Schwank − *Department of Chemical Engineering, University of Michigan, Ann Arbor, Michigan 48109, United States*; orcid.org/0000-0002-8218-5189; Email: schwank@umich.edu

Neil P. Dasgupta − *Department of Mechanical Engineering and Department of Materials Science and Engineering, University of Michigan, Ann Arbor, Michigan 48109, United States*; orcid.org/0000-0002-5180-4063; Email: ndasgupt@umich.edu

Authors

Alondra M. Ortiz-Ortiz − *Department of Mechanical Engineering, University of Michigan, Ann Arbor, Michigan 48109, United States*; orcid.org/0009-0004-4312-4449

Carissa S. Yim − *Department of Chemical Engineering, University of Michigan, Ann Arbor, Michigan 48109, United States*; orcid.org/0000-0002-4076-9055

Daniel O. Delgado Cornejo − *Department of Materials Science and Engineering, University of Michigan, Ann Arbor, Michigan 48109, United States*; orcid.org/0009-0002-3484-5960

Andrew J. Gayle − *Department of Mechanical Engineering, University of Michigan, Ann Arbor, Michigan 48109, United States*

Alexander J. Hill − *Department of Chemical Engineering, University of Michigan, Ann Arbor, Michigan 48109, United States*; orcid.org/0000-0003-0181-7920

Victor A. Vogt − *Department of Materials Science and Engineering, University of Michigan, Ann Arbor, Michigan 48109, United States*; orcid.org/0000-0002-9298-8401

Daniel W. Liao − *Department of Mechanical Engineering, University of Michigan, Ann Arbor, Michigan 48109, United States*

Thomas Coons − *Department of Mechanical Engineering, University of Michigan, Ann Arbor, Michigan 48109, United States*

Complete contact information is available at: https://pubs.acs.org/10.1021/acs.jpcc.4c05724

Author Contributions

[‖]A.M.O.-O. and C.S.Y. contributed equally to this work.

Notes

The authors declare no competing financial interest.

ACKNOWLEDGMENTS

This work was supported by the National Science Foundation through their Emerging Frontiers in Research and Innovation program (award number: 2131709). A.M.O.-O., C.S.Y., A.J.G., and T. C. acknowledge support from the National Science Foundation Graduate Research Fellowship Program under Grant No. DGE 1841052. The authors thank Jacob Hoffman for contributions to the reactor design, Anna R. Klinger for contributions to catalyst synthesis, and Prof. Rebecca D. Hardin for valuable feedback during the writing and editing process.

REFERENCES

(1) Chen, C.; Khosrowabadi Kotyk, J. F.; Sheehan, S. W. Progress toward Commercial Application of Electrochemical Carbon Dioxide Reduction. *Chem* **2018**, *4* (11), 2571−2586.

(2) Stangeland, K.; Kalai, D.; Li, H.; Yu, Z. CO2Methanation: The Effect of Catalysts and Reaction Conditions. *Energy Procedia* **2017**, *105*, 2022−2027.

(3) Kim, A.; Sanchez, C.; Haye, B.; Boissière, C.; Sassoye, C.; Debecker, D. P. Mesoporous TiO2 Support Materials for Ru-Based CO2Methanation Catalysts. *ACS Appl. Nano Mater.* **2019**, *2* (5), 3220−3230.

(4) Mateo, D.; Albero, J.; García, H. Photoassisted Methanation Using Cu 2 O Nanoparticles Supported on Graphene as a Photocatalyst. *Energy Environ. Sci.* **2017**, *10* (11), 2392−2400.

(5) Tripodi, A.; Conte, F.; Rossetti, I. Carbon Dioxide Methanation: Design of a Fully Integrated Plant. *Energy Fuels* **2020**, *34* (6), 7242−7256.

(6) Ran, J.; Jaroniec, M.; Qiao, S.-Z. Cocatalysts in Semiconductor-based Photocatalytic CO2 Reduction: Achievements, Challenges, and Opportunities. *Adv. Mater.* **2018**, *30* (7), 1704649.

(7) Guo, Q.; Zhou, C.; Ma, Z.; Yang, X. Fundamentals of TiO2 Photocatalysis: Concepts, Mechanisms, and Challenges. *Adv. Mater.* **2019**, *31* (50), 1901997.

(8) Yamada, Y.; Kanemitsu, Y. Determination of Electron and Hole Lifetimes of Rutile and Anatase TiO2 Single Crystals. *Appl. Phys. Lett.* **2012**, *101* (13), 133907.

(9) Habisreutinger, S. N.; Schmidt-Mende, L.; Stolarczyk, J. K. Photocatalytic Reduction of CO2 on TiO2 and Other Semiconductors. *Angew. Chem., Int. Ed.* **2013**, *52* (29), 7372−7408.

(10) Marszewski, M.; Cao, S.; Yu, J.; Jaroniec, M. Semiconductor-Based Photocatalytic CO 2 Conversion. *Mater. Horiz.* **2015**, *2* (3), 261−278.

(11) Ulmer, U.; Dingle, T.; Duchesne, P. N.; Morris, R. H.; Tavasoli, A.; Wood, T.; Ozin, G. A. Fundamentals and Applications of Photocatalytic CO2Methanation. *Nat. Commun.* **2019**, *10* (1), 3169.

(12) Fu, Y.; Li, J.; Li, J. Metal/Semiconductor Nanocomposites for Photocatalysis: Fundamentals, Structures, Applications and Properties. *Nanomaterials* **2019**, *9* (3), 359.

(13) Yang, J.; Wang, D.; Han, H.; Li, C. Roles of Cocatalysts in Photocatalysis and Photoelectrocatalysis. *Acc. Chem. Res.* **2013**, *46* (8), 1900−1909.

(14) Li, K.; Peng, B.; Peng, T. Recent Advances in Heterogeneous Photocatalytic CO2 Conversion to Solar Fuels. *ACS Catal.* **2016**, *6* (11), 7485−7527.

(15) Shoji, S.; Yin, G.; Nishikawa, M.; Atarashi, D.; Sakai, E.; Miyauchi, M. Photocatalytic Reduction of CO2 by CuxO Nanocluster Loaded SrTiO3 nanorod thin film. *Chem. Phys. Lett.* **2016**, *658*, 309−314.

(16) Cargnello, M.; Montini, T.; Smolin, S. Y.; Priebe, J. B.; Delgado Jaén, J. J.; Doan-Nguyen, V. V. T.; McKay, I. S.; Schwalbe, J. A.; Pohl, M.-M.; Gordon, T. R.; et al. Engineering Titania Nanostructure to Tune and Improve Its Photocatalytic Activity. *Proc. Natl. Acad. Sci. U. S. A.* **2016**, *113* (15), 3966−3971.

(17) Lin, X.; Yang, K.; Si, R.; Chen, X.; Dai, W.; Fu, X. Photo-Assisted Catalytic Methanation of CO in H2-Rich Stream over Ru/TiO2. *Appl. Catal., B* **2014**, *147*, 585−591.

(18) Chai, S.; Men, Y.; Wang, J.; Liu, S.; Song, Q.; An, W.; Kolb, G. Boosting CO2Methanation Activity on Ru/TiO2 Catalysts by Exposing (001) Facets of Anatase TiO2. *J. CO2 Util.* **2019**, *33*, 242−252.

(19) Wang, K.; He, S.; Lin, Y.; Chen, X.; Dai, W.; Fu, X. Photo-Enhanced Thermal Catalytic CO2Methanation Activity and Stability over Oxygen-Deficient Ru/TiO2 with Exposed TiO2 {001} Facets: Adjusting Photogenerated Electron Behaviors by Metal-Support Interactions. *Chin. J. Catal.* **2022**, *43* (2), 391−402.

(20) Zhang, X.; Li, X.; Reish, M. E.; Zhang, D.; Su, N. Q.; Gutiérrez, Y.; Moreno, F.; Yang, W.; Everitt, H. O.; Liu, J. Plasmon-Enhanced Catalysis: Distinguishing Thermal and Nonthermal Effects. *Nano Lett.* **2018**, *18* (3), 1714−1723.
(21) Albero, J.; Garcia, H.; Corma, A. Temperature Dependence of Solar Light Assisted CO 2 Reduction on Ni Based Photocatalyst. *Top. Catal.* **2016**, *59*, 787−791.
(22) Uner, D.; Oymak, M. M. On the Mechanism of Photocatalytic CO2 Reduction with Water in the Gas Phase. Frigyes Solymosi's Spec. Issue Planar Model Syst. *Heterog. Catal.* **2012**, *181* (1), 82−88.
(23) Meng, X.; Wang, T.; Liu, L.; Ouyang, S.; Li, P.; Hu, H.; Kako, T.; Iwai, H.; Tanaka, A.; Ye, J. Photothermal Conversion of CO2 into CH4 with H2 over Group VIII Nanocatalysts: An Alternative Approach for Solar Fuel Production. *Angew. Chem., Int. Ed.* **2014**, *53* (43), 11478−11482.
(24) Kim, C.; Hyeon, S.; Lee, J.; Kim, W. D.; Lee, D. C.; Kim, J.; Lee, H. Energy-Efficient CO2 Hydrogenation with Fast Response Using Photoexcitation of CO2 Adsorbed on Metal Catalysts. *Nat. Commun.* **2018**, *9* (1), 3027.
(25) Kawamura, S.; Zhang, H.; Tamba, M.; Kojima, T.; Miyano, M.; Yoshida, Y.; Yoshiba, M.; Izumi, Y. Efficient Volcano-Type Dependence of Photocatalytic CO2 Conversion into Methane Using Hydrogen at Reaction Pressures up to 0.80 MPa. *J. Catal.* **2017**, *345*, 39−52.
(26) Chen, Y.; Zhang, Y.; Fan, G.; Song, L.; Jia, G.; Huang, H.; Ouyang, S.; Ye, J.; Li, Z.; Zou, Z. Cooperative Catalysis Coupling Photo-/Photothermal Effect to Drive Sabatier Reaction with Unprecedented Conversion and Selectivity. *Joule* **2021**, *5* (12), 3235−3251.
(27) Zhang, Z.; Wang, Z.; Cao, S.-W.; Xue, C. Au/Pt Nanoparticle-Decorated TiO2 Nanofibers with Plasmon-Enhanced Photocatalytic Activities for Solar-to-Fuel Conversion. *J. Phys. Chem. C* **2013**, *117* (49), 25939−25947.
(28) Sastre, F.; Versluis, C.; Meulendijks, N.; Rodriguez-Fernandez, J.; Sweelssen, J.; Elen, K.; Van Bael, M. K.; den Hartog, T.; Verheijen, M. A.; Buskens, P. Sunlight-Fueled, Low-Temperature Ru-Catalyzed Conversion of CO2 and H2 to CH4 with a High Photon-to-Methane Efficiency. *ACS Omega* **2019**, *4* (4), 7369−7377.
(29) Petala, A.; Panagiotopoulou, P. Methanation of CO2 over Alkali-Promoted Ru/TiO2 Catalysts: I. Effect of Alkali Additives on Catalytic Activity and Selectivity. *Appl. Catal., B* **2018**, *224*, 919−927.
(30) Schneider, J.; Matsuoka, M.; Takeuchi, M.; Zhang, J.; Horiuchi, Y.; Anpo, M.; Bahnemann, D. W. Understanding TiO2 Photocatalysis: Mechanisms and Materials. *Chem. Rev.* **2014**, *114* (19), 9919−9986.
(31) Peiris, S.; de Silva, H. B.; Ranasinghe, K. N.; Bandara, S. V.; Perera, I. R. Recent Development and Future Prospects of TiO2 Photocatalysis. *J. Chin. Chem. Soc.* **2021**, *68* (5), 738−769.
(32) Dhakshinamoorthy, A.; Navalon, S.; Corma, A.; Garcia, H. Photocatalytic CO 2 Reduction by TiO 2 and Related Titanium Containing Solids. *Energy Environ. Sci.* **2012**, *5* (11), 9217−9233.
(33) Lorber, K.; Djinović, P. Accelerating Photo-Thermal CO2 Reduction to CO, CH4 or Methanol over Metal/Oxide Semiconductor Catalysts. *iScience* **2022**, *25* (4), 104107.
(34) Zhang, Y.; Su, X.; Li, L.; Qi, H.; Yang, C.; Liu, W.; Pan, X.; Liu, X.; Yang, X.; Huang, Y.; Zhang, T. Ru/TiO 2 Catalysts with Size-Dependent Metal/Support Interaction for Tunable Reactivity in Fischer−Tropsch Synthesis. *ACS Catal.* **2020**, *10* (21), 12967−12975.
(35) Rynkowski, J. M.; Paryjczak, T.; Lewicki, A.; Szynkowska, M. I.; Maniecki, T. P.; Jóźwiak, W. K. Characterization of Ru/CeO2-Al2O3 Catalysts and Their Performance in CO2Methanation. *React. Kinet. Catal. Lett.* **2000**, *71*, 55−64.
(36) Westrich, T. A.; Dahlberg, K. A.; Kaviany, M.; Schwank, J. W. High-Temperature Photocatalytic Ethylene Oxidation over TiO2. *J. Phys. Chem. C* **2011**, *115* (33), 16537−16543.
(37) Anouar, A.; García-Aboal, R.; Atienzar, P.; Franconetti, A.; Katir, N.; El Kadib, A.; Primo, A.; Garcia, H. Remarkable Activity of 002 Facet of Ruthenium Nanoparticles Grown on Graphene Films on the Photocatalytic CO2Methanation. *Adv. Sustain. Syst.* **2022**, *6* (5), 2100487.
(38) Tahir, M.; Amin, N. S. Performance Analysis of Nanostructured NiO−In2O3/TiO2 Catalyst for CO2 Photoreduction with H2 in a Monolith Photoreactor. *Chem. Eng. J.* **2016**, *285*, 635−649.
(39) Paulista, L. O.; Ferreira, A. F. P.; Castanheira, B.; Đolić, M. B.; Martins, R. J. E.; Boaventura, R. A. R.; Vilar, V. J. P.; Silva, T. F. C. V. Solar-Driven Thermo-Photocatalytic CO2Methanation over a Structured RuO2: TiO2/SBA-15 Nanocomposite at Low Temperature. *Appl. Catal., B* **2024**, *340*, 123232.
(40) Peng, Y.; Albero, J.; Franconetti, A.; Concepción, P.; García, H. Visible and NIR Light Assistance of the N2 Reduction to NH3 Catalyzed by Cs-Promoted Ru Nanoparticles Supported on Strontium Titanate. *ACS Catal.* **2022**, *12* (9), 4938−4946.
(41) Bielinski, A. R.; Gayle, A. J.; Lee, S.; Dasgupta, N. P. Geometric Optimization of Bismuth Vanadate Core−Shell Nanowire Photoanodes Using Atomic Layer Deposition. *ACS Appl. Mater. Interfaces* **2021**, *13* (44), 52063−52072.
(42) Li, L.; Zeng, W.; Song, M.; Wu, X.; Li, G.; Hu, C. Research Progress and Reaction Mechanism of CO2Methanation over Ni-Based Catalysts at Low Temperature: A Review. *Catalysts* **2022**, *12* (2), 244.
(43) Ashok, J.; Pati, S.; Hongmanorom, P.; Tianxi, Z.; Junmei, C.; Kawi, S. A Review of Recent Catalyst Advances in CO2Methanation Processes. *Catal. Today* **2020**, *356*, 471−489.
(44) Dongapure, P.; Bagchi, S.; Mayadevi, S.; Devi, R. N. Variations in Activity of Ru/TiO2 and Ru/Al2O3 Catalysts for CO2 Hydrogenation: An Investigation by in-Situ Infrared Spectroscopy Studies. *Mol. Catal.* **2020**, *482*, 110700.
(45) Hadjiivanov, K.; Lamotte, J.; Lavalley, J.-C. FTIR Study of Low-Temperature CO Adsorption on Pure and Ammonia-Precovered TiO2 (Anatase). *Langmuir* **1997**, *13* (13), 3374−3381.
(46) Kang, H.; Zhu, L.; Li, S.; Yu, S.; Niu, Y.; Zhang, B.; Chu, W.; Liu, X.; Perathoner, S.; Centi, G.; et al. Generation of Oxide Surface Patches Promoting H-Spillover in Ru/(TiO x) MnO Catalysts Enables CO2 Reduction to CO. *Nat. Catal.* **2023**, *6* (11), 1062−1072.
(47) Qin, X.; Xu, M.; Guan, J.; Feng, L.; Xu, Y.; Zheng, L.; Wang, M.; Zhao, J.-W.; Chen, J.-L.; Zhang, J.; et al. Direct Conversion of CO and H2O to Hydrocarbons at Atmospheric Pressure Using a TiO2−x/Ni Photothermal Catalyst. *Nat. Energy* **2024**, *9*, 154−162.

https://doi.org/10.1021/acs.jpcc.4c05724
J. Phys. Chem. C 2024, 128, 18284−18292